

1-1-2012

How to achieve maximum charge carrier loading on heteroatom-substituted graphene nanoribbon edges: Density functional theory study

Ting Liao
The University Of Queensland

Chenghua Sun
University of Queensland

Ziqi Sun
University of Wollongong, ziqi@uow.edu.au

Aijun Du
The University of Queensland

Denisa Hulicova-Jurcakova
University of Queensland

See next page for additional authors

Follow this and additional works at: <https://ro.uow.edu.au/engpapers>



Part of the [Engineering Commons](#)

<https://ro.uow.edu.au/engpapers/4850>

Recommended Citation

Liao, Ting; Sun, Chenghua; Sun, Ziqi; Du, Aijun; Hulicova-Jurcakova, Denisa; and Smith, Sean C.: How to achieve maximum charge carrier loading on heteroatom-substituted graphene nanoribbon edges: Density functional theory study 2012, 13751-13755.
<https://ro.uow.edu.au/engpapers/4850>

Authors

Ting Liao, Chenghua Sun, Ziqi Sun, Aijun Du, Denisa Hulicova-Jurcakova, and Sean C. Smith

How to achieve maximum charge carrier loading on heteroatom-substituted graphene nanoribbon edges: density functional theory study†

Ting Liao,^a Chenghua Sun,^{ab} Ziqi Sun,^c Aijun Du,^a Denisa Hulicova-Jurcakova^b and Sean C. Smith^{*d}

Received 8th March 2012, Accepted 3rd May 2012

DOI: 10.1039/c2jm31445b

The practical number of charge carriers loaded is crucial to the evaluation of the capacity performance of carbon-based electrodes in service, and cannot be easily addressed experimentally. In this paper, we report a density functional theory study of charge carrier adsorption onto zigzag edge-shaped graphene nanoribbons (ZGNRs), both pristine and incorporating edge substitution with boron, nitrogen or oxygen atoms. All edge substitutions are found to be energetically favorable, especially in oxidized environments. The maximal loading of protons onto the substituted ZGNR edges obeys a rule of $[8-n-1]$, where n is the number of valence electrons of the edge-site atom constituting the adsorption site. Hence, a maximum charge loading is achieved with boron substitution. This result correlates in a transparent manner with the electronic structure characteristics of the edge atom. The boron edge atom, characterized by the most empty p band, facilitates more than the other substitutional cases the accommodation of valence electrons transferred from the ribbon, induced by adsorption of protons. This result not only further confirms the possibility of enhancing charge storage performance of carbon-based electrochemical devices through chemical functionalization but also, more importantly, provides the physical rationale for further design strategies.

1. Introduction

Graphene is a flat monolayer of carbon atoms tightly packed into a honeycomb lattice. Its unique characteristics as a two-dimensional material have stimulated widespread efforts to gain a full understanding of its various properties through experimental and theoretical methods.^{1–6} Potential applications in condensed matter physics and electrochemistry have in particular highlighted a need to understand the structure and properties of its open edges,^{7–12} which are expected to display intrinsically different electronic features compared with other sp^2 based carbon-based nanostructures. In particular, the reactivity of zigzag edge-shaped graphene nanoribbons (ZGNRs) is very high due to the presence of highly localized electronic states at the

edge carbon atoms.^{13–15} For example, it is well documented that carbon atoms at the edges of ZGNRs offer superior chemical reactivity for the attachment of chemical groups than those on AGNR edges, in the ribbon's bulk, or on CNT edges.^{16,17}

Modification of nanoribbons by the introduction of appropriate elements or functional groups may enable the manipulation of electronic, structural and chemical properties, allowing targeting of different applications. In this context, the heteroatom substitutional doping and chemical functionalization have become topics of interest in sensing, transport, electrochemical and optical applications.^{18–25} The mechanism of energy storage in diverse electrochemical devices inherently involves movement of charge carriers to and from electrode surfaces. Thanks to the highly extended surface areas and excellent conductivity, chemically modified graphenes are currently the most extensively examined and widely utilized electrode materials, with development focusing on achieving a high adsorption concentration of charge carriers.^{21,24–27} The maximization of the concentration of charge carriers is decisive to determine the overall electrochemical performance of electrode. In contrast to the limitation of experiments, the edge chemistry of graphene ribbons can be more easily tailored using theoretical calculations. Consequently, studies of proton adsorption on chemically modified graphene ribbons at an electronic scale are extremely important and will provide a means for obtaining a rigorous theoretical understanding of the reactivity of charge carriers at a graphene electrode, a process of importance to fields as diverse as solutions, fuel-cell operation, and supercapacitors.

^aCentre for Computational Molecular Science, Australian Institute for Bioengineering and Nanotechnology, University of Queensland, Brisbane QLD4072, Australia. E-mail: t.liao1@uq.edu.au; c.sun1@uq.edu.au; a.du@uq.edu.au; Fax: +61 7 3346 3992; Tel: +61 7 3346 3972

^bARC Centre of Excellence for Functional Nanomaterials, Australian Institute for Bioengineering and Nanotechnology, University of Queensland, Brisbane QLD 4072, Australia. E-mail: c.sun1@uq.edu.au; d.jurcakova@uq.edu.au; Fax: +61 7 3346 3973; Tel: +61 7 3346 3830

^cInstitute for Superconducting & Electronic Materials, University of Wollongong, NSW 2500, Australia. E-mail: ziqi@uow.edu.au; Fax: +61 2 42215731; Tel: +61 2 42981479

^dCentre for Nanophase Materials Sciences, Oak Ridge National Laboratory, Oak Ridge, TN 37831, USA. E-mail: smithsc@ornl.gov; Fax: +1 865 574 1753; Tel: +1 865 574 5081

† Electronic supplementary information (ESI) available. See DOI: 10.1039/c2jm31445b

Theoretical electronic structures of GNRs have been extensively investigated using the tight-binding (TB) method and the *ab initio* density-functional theory (DFT) method.^{28–31} Density functional theory has long been proven as an effective method for the study of ground state properties of materials, and it has been applied extremely successfully to the calculation of physical, mechanical, and electrical properties in metal, semiconductor, and ionic conductors. Even though density functional theory has been criticized for poor evaluation of the band gap, for the present it is still the most widely adopted and highly recognized efficient *ab initio* method. More accurate methods (but much more time-consuming), such as the improved functional, orbital-dependent potentials, many-body correction, *etc.*, are preferred in further studies on the electronic properties of graphene nanoribbon systems if precise values are desired.^{32–36} Here, adopting first-principles electronic structure calculations, we report the band gap tuning of zigzag-shaped nanoribbons by edge doping, and also the maximal proton loading. Aside from identifying that the adsorption energy of protons is energetically favorable, we also arrive at the novel conclusion that the maximum numbers of adsorbed protons on each substituted ZGNR edge obey the rule of $[8-n-1]$ (n is the number of outermost valence electrons of the edge atom). (Explicit water molecules are also introduced in the supercell models to examine the effect of hydrogen bonds on proton adsorption on each substituted ribbon edge, and this does not change the conclusion.)

2. Computational methods

Our first-principles calculations are based on density-functional theory (DFT) with the Perdew–Burke–Ernzerhof gradient corrected functional,³⁷ as implemented in the PWSCF package.³⁸ Spin-polarized calculations are necessary for precise estimation of the energy of the open shell case in DFT, such as in the pristine and oxygen-substituted ribbons. In our case, however, the reduction of the predicted total energy by imposing spin polarization was found to be negligible. We used an ultrasoft pseudopotential to replace the core electrons of atoms.³⁹ In all calculations, a $7 \times 1 \times 1$ shifted Monkhorst–Pack⁴⁰ k -point mesh was used for the sampling of the Brillouin zone and a plane-wave cutoff energy of 40 Ry was used for the energy calculations to achieve a full convergence of 2×10^{-2} eV on total energies. A denser k -point grid of $15 \times 1 \times 1$ and a higher cutoff energy of 70 Ry were also adopted for testing, and the calculated total energy difference was no larger than 3×10^{-2} eV per atom, which suggests that the current parameters are sufficient to achieve a well-converged result. Geometry optimization procedures have been performed by fully relaxing the positions of all of the atoms in a supercell until the residual forces were smaller than 2.6×10^{-2} eV \AA^{-1} . Geometry optimization is performed for all of the structures with the Broyden–Fletcher–Goldfarb–Shanno algorithm.⁴¹

The unit cell of ZGNRs, as shown in the dashed line in Fig. 1a, is built from the perfect graphite geometry with an optimized periodic C–C bond distance of 4.274 \AA . We focused on a semi-infinite model by using a $3 \times 1 \times 1$ supercell, which is three times larger than the unit cell along the x -axis. The edge dangling bonds on the lower side of the nanoribbon are saturated with hydrogen atoms. In order to quench the formation of edge states and avoid unphysically low coordination numbers, the dangling

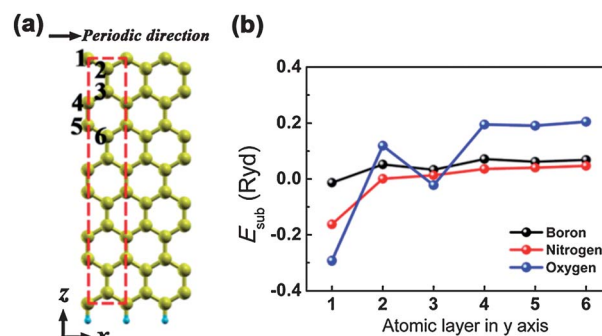


Fig. 1 (a) Scheme of $3 \times 1 \times 1$ eight-layer ZGNR supercell with a single edge H-saturated. The unit cell is indicated by the red dashed line; (b) plot of substitution energies of heteroatoms on carbon atoms at different layers as indicated by the number in (a).

bonds on the upper side, except for the ones involved in adsorbing protons, are also saturated. The in-plane and perpendicular distances between ribbons in adjacent supercells are as large as 10 and 15 \AA , respectively, creating sufficient vacuum to avoid the interactions between the adjacent supercells. In the proton adsorption calculations, a specific charge is assigned to the supercell. A neutralizing homogeneous background charge was assumed to avoid the divergence of the long-range interaction between the proton and its periodic images.

3. Results and discussions

3.1. Structural stability of heteroatom-doped nanoribbons

We began by investigating the substitutional stability of heteroatoms B, N, and O under dilute conditions. To simulate an isolated substitution center, our nanoribbon is described by a supercell using $3 \times 1 \times 1$ unit cells (Fig. 1a), implying that a substituted atom corresponds to an elemental concentration of 2.13%. The substitution energy can be addressed as

$$E_{\text{sub}} = E_{\text{heteroatom:ZGNR}} - E_{\text{ZGNR}} - \mu_{\text{heteroatom}} + \mu_{\text{carbon}} \quad (1)$$

where $E_{\text{heteroatom:ZGNR}}$ is the energy of the heteroatom-substituted supercell, E_{ZGNR} is the energy of pristine supercell, and $\mu_{\text{heteroatom}}$ and μ_{carbon} are calculated using the total energy of the ground states of each species. The site-specific substitution energies of heteroatoms starting from the edge and moving towards the inside layers of the ribbons are shown in Fig. 1b. The substitution is clearly most stable along the edge sites of the ribbons in all cases, with the energy difference to the inside layer site being larger than 0.9 eV per cell, which agrees well with the computational findings reported by Yu *et al.*⁴² Edges on graphene sheets can be viewed as topological defects, thus having electronic properties that are remarkably different from those of the inner sites. Scanning tunneling microscopy (STM) images of graphene sheets revealed bright stripes along their edges, suggesting a high density of edge states near the Fermi level.¹³ Another reason for this large substitution energy difference could be that the less constrained crystal lattice environment at the edge gives flexibility for more adequate geometrical relaxation to relieve strain induced by the substitution. For example, the largest atomic displacement during structural relaxation in the

boron edge-substituted supercell is more than 1.4 times greater than that occurring for the inner substitutions.

Effects related to varying the substitution ratio are considered by changing the size of the cell. The substitution stability was studied at two ratios, 2.13% and 6.67%. The doped atomic percentage of 2.13% corresponds to one dopant atom per $3 \times 1 \times 1$ supercell and 6.67% is one dopant atom per $1 \times 1 \times 1$ unit cell. In both cases substitution is only at the edge sites. As shown in Fig. 2, the substitution energies change only slightly when increasing the substitution ratio in this way for both B and N, implying no significant energetic interaction between the co-substituted heteroatoms. In the case of oxygen substitution, a repulsive interaction is observed between oxygen atoms in neighbors. All substitutional processes turn out to be exothermic, most notably for oxygen, which provides a complementary understanding of the easy contamination of graphene in oxidized environments.

3.2. Edge doping for band gap tuning in nanoribbons

The electronic structure of these heteroatom-substituted graphene nanoribbons is examined at the atomic percentage doping of 6.67% within the unit cell geometry (Fig. 3 and S1†), in order to investigate the intrinsic electronic mechanism responsible for the edge properties. In Fig. 3, we show the band structures of pristine ZGNR in comparison with B, N and O substitutional configurations. In the pristine ZGNR, the bare edge C atom has one orbital not participating in sp^2 hybridization. As a consequence, except for the metallic eigenstates ruled by edge π and π^* orbitals along wave vectors parallel to the x direction, the linear combinations of dangling bonds at the edges also form a flat σ band as expected near the Fermi energy, as shown in Fig. 3b. Because the mirror symmetry of both edges is broken in our semi-infinite

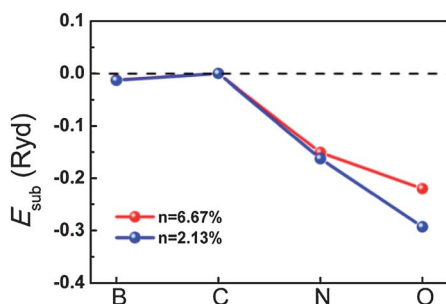


Fig. 2 Substitution energies of heteroatoms on the edge of ZGNRs considering different ratios.

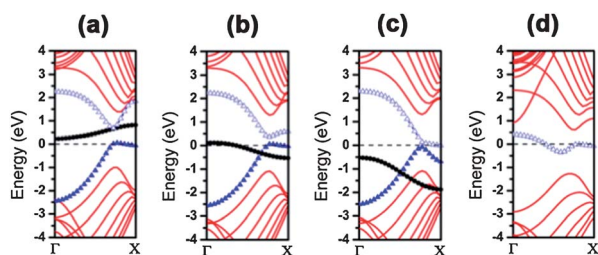


Fig. 3 Band structures of (b) pristine and (a), (c) and (d) edge-substituted ZGNR by B, N and O, respectively, triangles and circles indicate π - and σ -bands, respectively.

model, another electronic feature previously reported for symmetric models is no longer retained, namely, the flat π -top and π^* -bottom bands near the X point are no longer degenerate.

Since the unique properties of the ribbons are associated with their edge states, edge modification by replacing the edge C atom with another heteroatom – in the present study B, N or O – may facilitate control of the electronic structure properties of the ribbons. From Fig. 3a, c and d, it is apparent that B, N and O modify the electronic structure of pristine ribbons in the vicinity of the Fermi level such that B acts as an acceptor while N and O act as donors. Since no other states are formed in the band, the extra hole or electron coming from the doped element must be allocated in what were the initial valence or conduction bands of the pristine ribbon, with a consequent shift of the bands.

Upon boron edge substitution, as shown in Fig. 3a, the flat π band remains half occupied and constitutes the top of the valence band, whereas the σ band shifts upward to be above the Fermi energy and is therefore unoccupied. Hence, nanoribbons terminated with boron at the edge display an energy split between the π - π^* levels in equilibrium, as has also been very recently found by Martins.³¹ We find that in N substituted ribbons (Fig. 3c), the π - π^* states are perturbed only slightly and both the π band and the σ band are now fully occupied due to the extra electrons donated by the edge N atom. N-doped ZGNRs also give rise to a gapped semiconducting ribbon, although the gap energy is as small as 0.07 eV. In contrast, the oxygen-doped ribbon displays metallic character. The computational description of the graphene nanoribbon within density functional theory (DFT) is more or less straightforward. Since electronic exchange is nonlocal, while electronic interaction is described by the PBE potential under the generalized gradient approximation (GGA) in this work, the band gap is expected to be underestimated due to the semi-local approximation in the PBE potential, or due to the approximation resulted delocalization error. Nevertheless, most of the recent DFT calculations yield a description of this material in close accordance with experimental findings, quite independent of the exchange-correlation functional employed. Due to the large chemical potential difference induced by the substituted O atom, the O- p_x/p_z lone pair related fully occupied π - σ bands shift downward to lower energy ranges that are out of our examined range. Consequently, as shown in Fig. 3d, only the dispersive π^* band crosses the Fermi level.

3.3. Maximal proton loading on the doped edge of nanoribbons

Having studied the equilibrium geometry and electronic structure properties of heteroatom substitution on the exposed ribbon edge, we next examined their affiliation to charge carriers, *i.e.*, protons, within the finite supercells. The intrinsic dangling bonds at the ribbon edges provide active sites for chemical bonding and thus make the ribbons also suitable as a trap for attracting charge carriers. Our modeling setup considers ionized H (H^+) atoms as charge carriers. The adsorption energy was estimated by the total energy difference

$$E_{\text{ads}} = (E_{H^+\text{-edge}} - E_{\text{edge}} - n\mu_H)/n \quad (2)$$

where $E_{H^+\text{-edge}}$ is the total energy of ribbon with proton loading, E_{edge} is the energy of the bare ribbon with different heteroatom

substitution, μ_{H^+} is the chemical potential of a proton, and n is the number of loaded protons. In an aqueous source H^+ is in the ionized state, hence μ_{H^+} can be calculated as the total energy of positively charged H in a sufficiently large supercell. Further details on the theoretical methods are given in ref. (43–46).

The adsorption of protons on the (bare) heteroatom-substituted edge of ZGNRs has also been investigated with regard to maximum loading and consequently the protonic charge carrier density available. As shown in Fig. 4, the adsorption of protons is exothermic, revealing that the adsorption of pre-existing protons onto the edge of ZGNRs is strongly energetically favorable up to a certain maximal loading. Total energy results also indicate that there is a repulsive interaction between the co-adsorbed charge carriers, such that the single adsorption configuration is energetically the most favorable as shown in Fig. 4 and the exothermic adsorption energy decreases gradually with more adsorbed protons. There exist limited computational and experimental results to date for the interaction energies of protons with bare graphene edges in an aqueous environment that would allow us to make a direct comparison. As shown in Fig. 4b, the number of protons that can be adsorbed onto the heteroatom-substituted edge of ZGNRs follows the rule of $8-n-1$, where 8 is the maximal occupation for the outermost $s+p$ orbitals (valence shell) and n is the number of valence electrons of the edge atom. This result is in close resemblance to the case of hydrogen atom adsorption on transition metal atoms, where the maximum number adsorbed has been reported to obey an 18-electron rule,⁴⁷ where the phenomenon is also intrinsically correlated with the outermost electronic structure characteristics of edge atoms. The present $8-n-1$ rule may be rationalized in terms of the observation that, in the absence of counter ions, coulomb repulsion will make it energetically unfavorable for two positive charges to be localized on a given edge site. Taking oxygen as a first example, its valence shell is already filled (through the two sigma bonds to its neighboring carbon atoms). Hence, the Lewis base properties of oxygen will allow one proton to adsorb, but a second adsorption onto the same oxygen site would be energetically unfavorable due to charge repulsion. Moving to nitrogen, which has one less valence electron, we note that it is possible to adsorb a second proton to the same nitrogen site because one electron can be drawn from the ribbon (most likely localized from within the π -framework) to the N adsorption site to facilitate attachment of the second proton, simultaneously dispersing the second positive charge over a larger area and thereby avoiding the coulomb repulsion barrier. This fills the

valence shell of the edge nitrogen atom. No further protons can be adsorbed onto that site since, with the N valence shell now filled, no more electrons can be localized from the ribbon and hence a third adsorbed proton would run into the energy barrier associated with repulsion between two localized positive charges. Following this same line of argument it becomes apparent why an edge carbon site can adsorb up to three protons (with two electrons localized from the ribbon until its valence shell is filled) and an edge boron atom can adsorb up to four protons (with three electrons localized from the ribbon until its valence shell is filled). Hence, the number of protons adsorbed will be maximized in the case of B-doped ZGNRs. This result gives a simple and transparent explanation of the experimental observation that boron-doped active carbon exhibits higher interfacial capacitance than that of boron-free carbon.⁴⁸

Next, we study the difference electron density (ρ_{diff}) isosurfaces in all the configurations at each proton loading in order to characterize the occurrence of charge-transfer processes and to identify which orbitals are involved in the bonding process. In the proton adsorbed nanoribbon system, ρ_{diff} is given by

$$\rho_{\text{diff}} = \rho(\text{H}^+\text{-edge}) - \rho(\text{H}^+) - \rho(\text{edge}) \quad (3)$$

where $\rho(\text{H}^+\text{-edge})$ is the electron density of a supercell containing the loaded proton nanoribbon system, $\rho(\text{H}^+)$ is the electron density of the same supercell with the proton only, and $\rho(\text{edge})$ is analogous for the nanoribbon system only. Thus, a ρ_{diff} isosurface indicates the charge displacements induced by an interaction between the proton and the active ribbon edge. We notice that the morphology of an adsorbed proton on the ribbon edge is independent of the type of edge atom. In all the cases here reported, the energetically favorable spatial arrangements of the adsorbed protons are within a plane perpendicular to the ribbon surface [see Fig. 5 and S2†]. A proton is a highly ionized particle and in most cases will act as an electron trap. Due to the strong electronegativity difference between the adsorbed proton and the edge atom, the calculated difference in charge distribution reveals that most charge transfer occurs from the partially or fully occupied ribbon edge atom- p orbitals to the adsorbed proton- s orbitals, and hence, as a result of electron polarization, a strong interaction forms between the adsorbed proton and the edge atom in every case. As shown in Fig. 5, the accumulation of charge in the adsorbed proton layer is highly localized and is characteristic of an s -orbital symmetry. It is worth noting that the proton adsorption mechanism shown in the above systems is mainly related to the electronic structure properties of the edge atoms, which are characterized by a variety of localized states

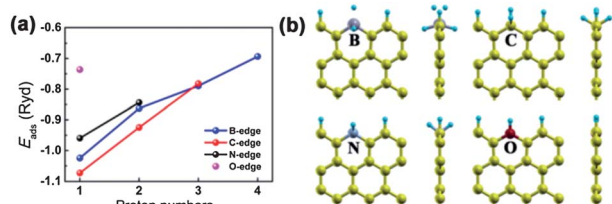


Fig. 4 (a) Calculated edge adsorption energies of protons on zigzag edge-shaped graphene nanoribbons as a function of the number of adsorbed protons. (b) Front and side views of the atomic configuration of doped ribbons with maximal numbers 4, 3, 2, and 1 of adsorbed protons for exposed B-, C-, N-, and O-edges respectively.

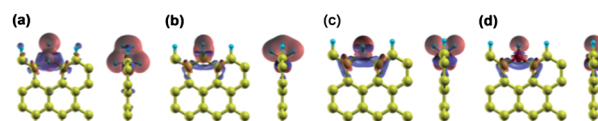


Fig. 5 Front and side views of the charge density difference of maximally loaded protonated ZGNRs with (b) pristine and heteroatom (a) boron, (c) nitrogen and (d) oxygen substituted ribbons (isovalues for all the isosurfaces are $\pm 0.005 \text{ e}\text{\AA}^{-3}$). Only the top several atomic layers are shown for better visualization. Red indicates electronic density gain, blue indicates electronic density loss.

near the Fermi level, *e.g.*, boron as a good electron acceptor is the one having the most empty orbitals, which facilitates the accommodation of more valence electrons (drawn from the ribbon) to spread the charge associated with adsorption of additional protons. The greater capacity for proton adsorption makes boron an attractive candidate for improving the charge and energy storage capability of edge-dominated carbon materials.

4. Conclusions

In conclusion, the capacity for uptake of adsorbed protons onto the heteroatom-substituted edge of zigzag-shaped graphene ribbons has been studied and the corresponding change of electronic structure characteristics analyzed using density functional theory calculations. For heteroatom B-, N-, and O-substituted ribbons, the energetically preferred substitution site is at the edge of each ribbon. All edge doping processes are exothermic in either a donor or acceptor way. The energy gain by heteroatom substitution is more significant when the dopant is a nitrogen or oxygen atom, which is helpful in explaining the ready contamination of graphene in oxidized environments. The consideration of substitution percentage using different sized models suggests an increasing amount of oxygen dopant at the ribbon edge could easily give rise to structural instability.

The adsorption of protons to the exposed ribbon edge is found to be strongly exothermic up to a certain maximal loading. The maximum number of adsorbed protons onto the substituted ZGNR edges depends on the type of dopant (4, 3, 2, and 1 for B, C, N, and O, respectively) and obeys a rule of $(8-n-1)$, where n is the number of valence electrons of the edge atoms. In other words, the B-doped ribbon edge accepts the largest number of protons amongst the cases studied here. This result leads to a better understanding at the electronic level of the adsorption mechanisms of charge carriers coupled with the edge chemistry of graphene ribbons, which is helpful to design high-performance carbon-based supercapacitor devices.

Acknowledgements

TL acknowledges financial support from the University of Queensland Postdoctoral Research Fellowship. We also appreciate the generous grants of CPU time from both the University of Queensland and the Australian National Computational Infrastructure Facility. SCS acknowledges support from the Center for Nanophase Materials Sciences, which is sponsored at the Oak Ridge National Laboratory by the Scientific User Facilities Division, US Department of Energy.

Notes and references

- C. N. R. Rao, A. K. Sood, K. S. Subrahmanyam and A. Govindaraj, *Angew. Chem., Int. Ed.*, 2009, **48**, 7752.
- S. A. Shevlin and Z. X. Guo, *Chem. Soc. Rev.*, 2009, **38**, 211.
- H. T. Liu, S. M. Ryu, Z. Y. Chen, M. L. Steigerwald, C. Nuckolls and L. E. Brus, *J. Am. Chem. Soc.*, 2009, **131**, 17099.
- C. L. Kane and E. J. Mele, *Phys. Rev. Lett.*, 2005, **95**, 226801.
- L. Shen, M. G. Zeng, S. W. Yang, C. Zhang, X. F. Wang and Y. P. Feng, *J. Am. Chem. Soc.*, 2010, **132**, 11481.
- K. S. Novoselov, A. K. Geim, S. V. Morozov, D. Jiang, Y. Zhang, S. V. Dubonos, I. V. Grigorieva and A. A. Firsov, *Science*, 2004, **306**, 666.
- L. A. Agapito and H. P. Cheng, *J. Phys. Chem. C*, 2007, **111**, 14266.
- K. A. Ritter and J. W. Lyding, *Nat. Mater.*, 2009, **8**, 235.
- D. Querlioz, Y. Apertet, A. Valentin, K. Huet, A. Bournel, S. Galdin-Retailleau and P. Dollfus, *Appl. Phys. Lett.*, 2008, **92**, 042108.
- S. N. Kim, Z. F. Kuang, J. M. Slocik, S. E. Jones, Y. Cui, B. L. Farmer, M. C. McAlpine and R. R. Naik, *J. Am. Chem. Soc.*, 2011, **133**, 14480.
- N. G. Shang, P. Papakonstantinou, M. McMullan, M. Chu, A. Stamboulis, A. Potenza, S. S. Dhesi and H. Marchetto, *Adv. Funct. Mater.*, 2008, **18**, 3506.
- M. Y. Han, B. Ozyilmaz, Y. Zhang and P. Kim, *Phys. Rev. Lett.*, 2007, **98**, 206805.
- Y. Kobayashi, K. I. Fukui, T. Enoki and K. Kusakabe, *Phys. Rev. B: Condens. Matter Mater. Phys.*, 2006, **73**, 125415.
- D. Klein, *Chem. Phys. Lett.*, 1994, **217**, 261.
- K. Nakada, M. Fujita, G. Dresselhaus and M. S. Dresselhaus, *Phys. Rev. B: Condens. Matter*, 1996, **54**, 17954.
- F. Cervantes-Sodi, G. Csányi, S. Piscanec and A. C. Ferrari, *Phys. Rev. B: Condens. Matter Mater. Phys.*, 2008, **77**, 165427.
- A. A. Balandin, S. Ghosh, W. Z. Bao, I. Calizo, D. Teweldebrhan, F. Miao and C. N. Lau, *Nano Lett.*, 2008, **8**, 902.
- R. Ruoff, *Nat. Nanotechnol.*, 2008, **3**, 10.
- Q. M. Yan, B. Huang, J. Yu, F. W. Zheng, J. Zang, J. Wu, B. L. Gu, F. Liu and W. H. Duan, *Nano Lett.*, 2007, **7**, 1469.
- D. Gunlycke, J. Li, J. W. Mintmire and C. T. White, *Appl. Phys. Lett.*, 2007, **91**, 112108.
- L. L. Zhang, R. Zhou and X. S. Zhao, *J. Mater. Chem.*, 2010, **20**, 5983.
- D. Chen, L. H. Tang and J. H. Li, *Chem. Soc. Rev.*, 2010, **39**, 3157.
- Y. Wang, X. H. Chen, Y. L. Zhong, F. R. Zhu and K. P. Loh, *Appl. Phys. Lett.*, 2009, **95**, 063302.
- V. Barranco, M. A. Lillo-Rodenas, A. Linares-Solano, A. Oya, F. Pico, J. Ibanez, F. Agullo-Rueda, J. M. Amarilla and J. M. Rojo, *J. Phys. Chem. C*, 2010, **114**, 10302.
- Y. Wang, Z. Q. Shi, Y. Huang, Y. F. Ma, C. Y. Wang, M. M. Chen and Y. S. Chen, *J. Phys. Chem. C*, 2009, **113**, 13103.
- V. C. Tung, M. J. Allen, Y. Yang and R. B. Kaner, *Nat. Nanotechnol.*, 2009, **4**, 25.
- S. F. Hou, M. L. Kasner, S. J. Su, K. Patel and R. Cuellari, *J. Phys. Chem. C*, 2010, **114**, 14915.
- D. H. Choe, J. Bang and K. J. Chang, *New J. Phys.*, 2010, **12**, 125005.
- J. H. Lan, J. S. Wang, C. K. Gan and S. K. Chin, *Phys. Rev. B: Condens. Matter Mater. Phys.*, 2009, **79**, 115401.
- S. Dutta, A. K. Manna and S. K. Pati, *Phys. Rev. Lett.*, 2009, **102**, 096601.
- T. B. Martins, R. H. Miwa, A. J. R. da Silva and A. Fazio, *Phys. Rev. Lett.*, 2007, **98**, 196803.
- P. Mori-Sánchez, A. J. Cohen and W. T. Yang, *Phys. Rev. Lett.*, 2008, **100**, 146401.
- A. J. Cohen, P. Mori-Sánchez and W. T. Yang, *Chem. Rev.*, 2012, **112**, 289.
- A. J. Cohen, P. Mori-Sánchez and W. T. Yang, *Science*, 2008, **321**, 792.
- S. Kümmel and L. Kronik, *Rev. Mod. Phys.*, 2008, **80**, 3.
- T. P. Lybrand and P. A. Peter, *J. Chem. Phys.*, 1985, **83**, 2923.
- J. P. Perdew, K. Burke and M. Ernzerhof, *Phys. Rev. Lett.*, 1996, **77**, 3865.
- S. Baroni, A. Dal Corso, S. de Gironcoli and P. Giannozzi, PWSCF (plane wave self consistent field) codes available at: <http://www.quantum-espresso.org>.
- D. Vanderbilt, *Phys. Rev. B: Condens. Matter*, 1990, **41**, 7892.
- J. D. Pack and H. J. Monkhorst, *Phys. Rev. B: Solid State*, 1977, **16**, 1748.
- B. G. Pfrommer, M. Côté, S. G. Louie and M. L. Cohen, *J. Comp. Physiol.*, 1997, **131**, 233.
- S. S. Yu, W. T. Zheng, Q. B. Wen and Q. Jiang, *Carbon*, 2008, **46**, 537.
- S. B. Zhang and J. E. Northrup, *Phys. Rev. Lett.*, 1991, **67**, 2339.
- A. D. Becke, *J. Chem. Phys.*, 1993, **98**, 1372.
- Q. Zhang, R. Bell and T. N. Truong, *J. Phys. Chem.*, 1995, **99**, 592.
- W. Koch and M. C. Holthausen, *A Chemist's Guide to Density Functional Theory*, Wiley-VCH Verlag GmbH, 2nd edn, 2001.
- D. M. P. Mingos, *J. Organomet. Chem.*, 2004, **689**, 4420.
- D. W. Wang, F. Li, Z. G. Chen, G. Q. Lu and H. M. Cheng, *Chem. Mater.*, 2008, **20**, 7195.